

LETTER TO THE EDITOR

A sub-Earth-mass planet orbiting Barnard's star

No evidence of transits in TESS photometry

A. K. Stefanov^{1,2,*}, J. I. González Hernández^{1,2}, A. Suárez Mascareño^{1,2}, N. Nari^{1,2,3}, R. Rebolo^{1,2,4}, M. Damasso⁵,
A. Castro-González⁶, M.-R. Zapatero Osorio⁶, C. Allende Prieto^{1,2}, A. M. Silva^{7,8,9}, C. J. A. P. Martins^{7,10}

(Affiliations can be found after the references)

October 2, 2024

ABSTRACT

A sub-Earth-mass planet orbiting Barnard's star, designated as Barnard b, has been recently announced. At a similar time, the first photometric data of Barnard's star by the Transit Exoplanet Survey Satellite (TESS) was released in Sector 80. We explore the possibility of emergent transits of Barnard b in TESS photometry. The detrended 2 min light curve appears to be flat, with a flux root-mean-square of 0.411 parts per thousand. Attempts of blind and informed transit-curve model inference suggest no evidence of transiting Barnard b, or any other body. This provides a 3σ upper bound of 87.9 degrees for the orbital inclination of Barnard b.

Key words. techniques: photometric – stars: low-mass – stars: individual: Barnard's star – stars: individual: HIP 87937 – stars: individual: GJ 699

1. Introduction

Exoplanetary astronomy has had a remarkable expansion in recent years. The number of confirmed exoplanets is soon to reach 5800 (NASA Exoplanet Archive, Akeson et al. 2013; accessed September 2024). Astronomers are already on track to discover potentially habitable Earth-like planets (e.g. Crossfield et al. 2015; Gillon et al. 2016; Murgas et al. 2023; Suárez Mascareño et al. 2023). The discovery of a planet in the habitable zone of Proxima, in the closest stellar system to our own (Proxima b; Anglada-Escudé et al. 2016), rocked the scientific community. It hinted that potential Earth analogues may lie in the very vicinity of the solar neighbourhood. Subsequently, considerable effort has been devoted to the analysis of such nearby systems. This led to a natural focus on the second closest stellar system: Barnard's star (Table 1), an M3.5V-M4V dwarf that has been thoroughly examined since its discovery (Barnard 1916).

Most recently, González Hernández et al. (2024), hereinafter GH24, reported the detection of a sub-Earth mass planet around Barnard's star. This planet, designated as Barnard b, has an orbital period $P_b = 3.1533 \pm 0.0006$ d and a minimum mass of $M_b \sin i_b = 0.37 \pm 0.05 M_\oplus$. The proximity of Barnard b to its host star (0.02 au) implies a transit probability of 3.7% – which in turn would offer an extraordinary opportunity for its atmospheric characterisation. The Transiting Exoplanet Survey Satellite (TESS; Ricker et al. 2015) had obtained photometric observations of Barnard's star between June and July 2024, and released those data as part of the Sector 80 (S80) data release in late August 2024 – a mere few days after the acceptance of GH24. The present Letter serves to extend their work by exploring potential transits of Barnard b in this new and only TESS photometry.

2. Data

SPOC provides with two different photometric data products: SAP and PDCSAP. SAP is a simple summation of flux from the

Table 1. Relevant parameters of Barnard's star.

Parameter	Symbol	Unit	Value	Ref.
Right ascension	α_{J2000}	–	$17^{\text{h}}57^{\text{m}}48.5^{\text{s}}$	2
Declination	δ_{J2000}	–	$+04^{\circ}41'36.1''$	2
Eff. temperature	T_{eff}	K	3195 ± 28	1
Mass	M_\star	M_\odot	0.162 ± 0.007	3
Radius	R_\star	R_\odot	0.185 ± 0.006	3
Surface gravity	$\log_{10} g$	cm s^{-2}	4.90 ± 0.09	1
Metallicity	[Fe/H]	dex	-0.56 ± 0.07	1

References. (1) González Hernández et al. (2024); (2) Gaia Collaboration et al. (2022); (3) Schweitzer et al. (2019).

optimal aperture of the target determined by SPOC. Its data may suffer from systematics of different nature, including: contamination from other sources, cosmic rays, variable incident solar radiation, foreign particles on CCD sensors and systematics from spacecraft motion. With a similar rationale, but regarding the Kepler mission, Kinemuchi et al. (2012) argued that SAP data should be expected to carry all these systematics; and analysis of subtle photometric variations on time-scales larger than 1 d is likely to be affected. PDCSAP, on the other hand, aims to mitigate signal artifacts and instrumental effects in SAP data. The basic mode of operation is described in the same work, Sect. 4.2; and has been further refined since then (see Stumpe et al. 2012; Smith et al. 2012; Stumpe et al. 2014). We discuss SAP and PDCSAP data in all analysis that follows.

We studied the origin of flux inside the SPOC aperture of Barnard's star through the TESS contamination tool TESS-CONT (Castro-González et al. 2024). We analysed the TESS pixel-response functions of all sources within 500 arcsec ($N = 4819$). We found that 99.5% of the aperture flux indeed comes from Barnard's star. The remaining 0.5% are ascribed to fainter

Table 2. Relevant parameters of Barnard b.

Symbol	Unit	Value	Ref.
a_b	au	0.02294(33)	1
P_b	d	3.1533(6)	1
$T_{0,b} - 2\,460\,000$	d	139.204 ± 0.149	1
$M_b \sin i_b$	M_\oplus	0.37 ± 0.05	1
R_b	R_\oplus	0.76 ± 0.04	0
D_b	ppt	$1.55^{+0.26}_{-0.28}$	0
W_b	h	$0.82^{+0.11}_{-0.27}$	0

References. (0) This work; (1) González Hernández et al. (2024).

Notes. The expected radius, transit depth and transit width were naïvely computed under two assumptions: (i) that Barnard b follows the mass-radius relation provided by Parviainen et al. (2024); (ii) that the impact parameter follows the uniform distribution $\mathcal{U}(0, 1)$. Reported uncertainties reflect the 16th and the 84th percentiles. Some uncertainties are given in parentheses, to the order of the least significant figure.

sources, whose small contributions add up to a negligible contamination.

3. Analysis

Two parameters define the general shape of a transit: the transit width W from first to fourth contact, and the transit depth D . Deriving some characteristic values of W and D , even if approximate, would give us clues when we look out for features in photometry. Both parameters, and especially D , are sensitive to the planetary radius R_b , which in the case of Barnard b is not directly probed in GH24. Nevertheless, we can relate their measured $M_b \sin i_b$ to R_b for an assumed mass-radius relation and an assumed impact-parameter distribution. We use the mass-radius relation provided by *SPRIGT* (Parviainen et al. 2024) to estimate R_b under the assumption $\sin i_b \approx 1$. For an impact-parameter distribution, we adopt $b = \mathcal{U}(0, 1)$, which would be implied by a random orbital orientation relative to the line of sight.

We then set out to estimate of W and D through rapid transit-curve modelling. We assumed that the limb-darkening profile of Barnard’s star follows the quadratic law

$$\frac{I(\vartheta)}{I(\vartheta = 0^\circ)} = 1 - u_1(1 - \cos \vartheta) - u_2(1 - \cos \vartheta)^2, \quad (1)$$

where I is the total emergent intensity, and ϑ is the angle between the line of sight and the direction of the emergent radiation (Kopal 1950). We fed stellar-parameter measurements from Table 1 to *LDTK* (Parviainen & Aigrain 2015; Husser et al. 2013), which returned $u_1 = 0.2470 \pm 0.0013$ and $u_2 = 0.3814 \pm 0.0026$ for the TESS passband. We then computed 10^6 transit curves from the distributions of: (i) $R_\star, M_\star, P_b, M_b$ from GH24; (ii) R_b from *SPRIGT*; (iii) u_1, u_2 from *LDTK*, assumed Gaussian; (iv) $b = \mathcal{U}(0, 1)$. We calculated W and D of each lightcurve individually, and we list their aggregate statistics together with our derived R_b in Table 2. The bulk of the distribution of R_b appeared Gaussian-like, with few outliers beyond $1 R_\oplus$. We expect a transit of depth $1.55^{+0.26}_{-0.28}$ ppt (points per thousand) and of duration $0.82^{+0.11}_{-0.27}$ h. GH24 provided with an additional four-planet solution that contains Barnard b and three planetary candidates; we repeat the same procedure for those solutions and list the corresponding results in Table A.1.

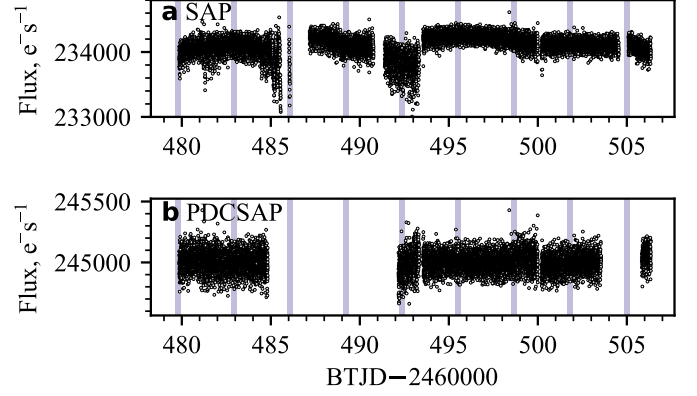


Fig. 1. TESS S80 photometric data products: (a) SAP, (b) PDCSAP, with superimposed predicted times of inferior conjunction through GH24 ephemerides. The propagated inferior-conjunction uncertainty is shown in light-blue bands.

3.1. Lack of features in TESS S80 data

We took all 2 min SAP and PDCSAP measurements from the TESS S80 lightcurve, using the default cadence quality bitmask. The SAP dataset is comprised of 16 492 measurements that span between 2 460 479–2 460 507 BTJD. SAP measurements have a root-mean-square (rms) of $166 \text{ e}^- \text{ s}^{-1}$ and a median uncertainty of $52 \text{ e}^- \text{ s}^{-1}$. We show these timeseries in Fig. 1a, together with predicted inferior conjunctions of Barnard b from GH24 ephemerides. SAP measurements are split in several portions, and contain irregular negative trends that tend to take place at the end of those portions (e.g. near 2 460 485 BTJD or 2 460 493 BTJD). Yet, there is no apparent evidence of a strictly periodic decrease in flux – which would be otherwise caused by the sought planetary transit. The PDCSAP timeseries share the same temporal span, but with 4691 excluded measurements in the interval 2 460 485–2 460 492 BTJD (Fig. 1b). This exclusion affected two predicted inferior conjunctions. PDCSAP timeseries contain 11 801 measurements that have a flux rms of $78.4 \text{ e}^- \text{ s}^{-1}$ and a median uncertainty of $54.5 \text{ e}^- \text{ s}^{-1}$.

We proceeded with SAP in an attempt to include data near the inferior-conjunction predictions that PDCSAP dismissed. We smoothed the SAP timeseries with several variants of detrending, including: second-order Savitzky-Golay filters (Savitzky & Golay 1964), Tukey’s biweight time-window sliders (Mosteller & Tukey 1977) and mean time-window sliders – all available in *WOTAN* (Hippke et al. 2019). We globally used a window length 0.5 d, an edge cut-off of 0.3 d and a break tolerance of 0.2 d. For none of these forms of detrending could we find evidence of transits after generating transit-least squares periodograms (TLSPs; Hippke & Heller 2019) or box-least squares periodograms (BLSPs; Kovács et al. 2002) for periodicities between 1–15 d and transit widths between 0.2–2 h.

We chose to go forward with mean time-window detrending by virtue of its simplicity. Figure 2 displays this detrended SAP photometry. It contains 14 366 measurements which are characterised by a flux rms of 0.411 ppt and a median uncertainty of 0.222 ppt. The flux rms is near four times smaller than the expected transit depth ($1.55^{+0.26}_{-0.28}$ ppt; Fig. 2). Figure 2a compares these processed timeseries again with the predicted inferior conjunctions of Barnard b from GH24. Six inferior conjunctions are covered by photometry within ephemeris precision. We could observe no significant decreases in flux at those ephemerides, or anywhere else. We folded the timeseries at the published period

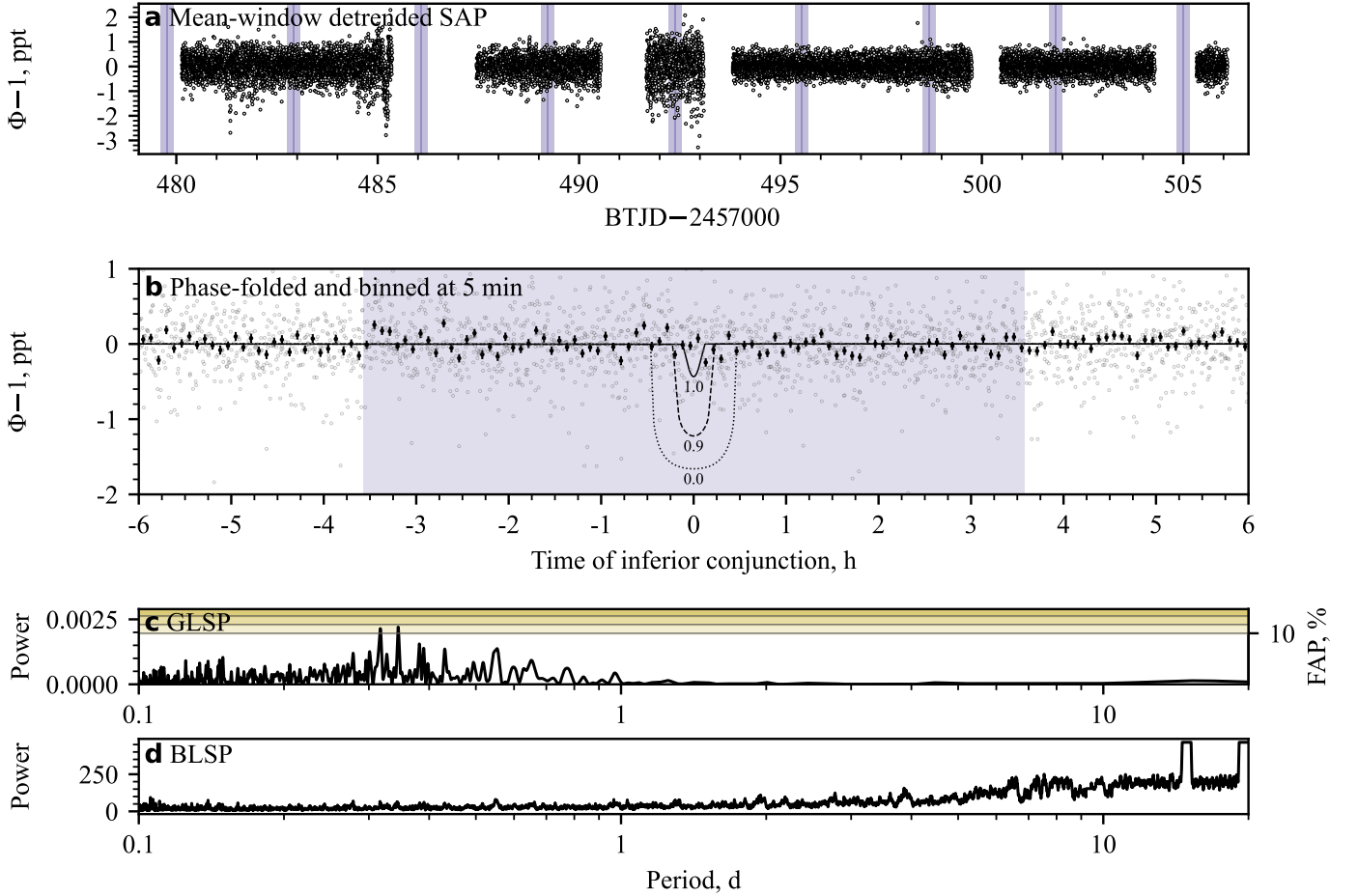


Fig. 2. (a) Mean time-window detrended SAP photometry with superimposed predicted times of inferior conjunction through GH24 ephemerides. The median expected duration of the transit is displayed in dark-blue bands. The propagated ephemeris uncertainty is shown in light-blue bands. (b) A phase-folded plot at GH24 ephemerides: before and after applying a 5 min binning (light hollow, and dark filled circles respectively). The inferior-conjunction epoch uncertainty is shown in a light-blue band. We compare photometry against the expected transit-curve of Barnard b for three impact-parameter values: $b = 0.0$ (black dotted line), $b = 0.9$ (black dashed line) and $b = 1.0$ (black solid line). (c) GLSP of unbinned data. (d) BLSP of unbinned data.

and epoch of Barnard b, and binned the phased data at 5 min. Figure 2b illustrates the result of this exercise, together with the epoch uncertainty and `PYTRANSIT` curves from the median posteriors of Table 2 for three impact-parameter values: 0, 0.9 and 1. Measurements do not evidently follow predictions for such a liberal range of impact parameters, regardless whether binning was involved or not. This remained the case after binning at other intervals (2–10 min). On the whole, these timeseries give an impression of notable symmetry and lack of apparent features, as if we observe pure noise when measuring a constant-flux source. The distribution of measurements is Gaussian-like, with right tail being asymmetrically heavier (Fig. A.1). On the other hand, transits must break the one-dimensional distribution symmetry in the opposite direction, i.e. they would give a heavy left tail.

3.2. Lack of plausible transit solutions

We performed transit-curve fitting through `PYTRANSIT` and nested sampling (Skilling 2004). For the inference of these models, we used the nested-sampling integrator provided by `DYNESTY` (Speagle 2020). In every inference instances with N_{param} model parameters, we required $40N_{\text{param}}$ live points and random-walks sampling. We modelled for one planet on a circular orbit, using GH24 ephemerides as priors. We imposed two different pri-

ors on the planetary radius: one informed by the expected radius ($\mathcal{N}(0.76, 0.04) R_{\oplus}$; Table 2), as well as one with the very uninformed $\mathcal{U}_{\log}(e^{-5}, e^{+5}) R_{\oplus}$, i.e. up to $148 R_{\oplus}$. Our impact-parameter prior was liberally set to $\mathcal{U}(0, 1.5)$. Quadratic limb-darkening coefficients were drawn from Gaussian distributions defined by `LDTK` given stellar parameters from Table 1. Their variances were scaled three-fold to ensure impartiality. All models sampled for a zero-order flux offset $\Delta\Phi$, and they included a rigid jitter component of 0.25 ppt, based on the rms of the first 10 d of data.

Bayesian evidences of one-planet models hint that data does not support a planetary addition ($\Delta \ln Z = -89$ for narrow R_b priors, $\Delta \ln Z = -143$ for wide R_b priors). The narrow-prior model restricts impact-parameter solutions to $b > 1$ (3σ), which correspond to inclinations $i_b < 87.9^\circ$ (Figure A.2). This goes on to suggest that data are not compatible with any transiting events with the properties of Barnard b, including cases of grazing transits. Although the wide-prior model provided upper limits to potential transiting planets, we note a large degeneracy between radius and inclination. For $i_b > 88^\circ$, planetary radii up to $0.3 R_{\oplus}$ were allowed. As soon as we crossed $i_b = 88^\circ$, sensitivity decreased to $2 R_{\oplus}$, and for $i_b < 87^\circ$ even $10 R_{\oplus}$ planets would remain undetected. We tested models with and without Gaussian processes (GPs; Rasmussen & Williams 2006), using a Matérn

5/2 kernel as defined in `s+LEAF` (Delisle et al. 2020, 2022). We additionally included three more planets in the model to try to reach the four-planet solution in GH24. The inclusion of neither GPs nor additional planets had no meaningful effect.

4. Conclusion

We investigated the first, and, to date, the only TESS sector, S80, that contains photometry of Barnard’s star. Photometry of all modes were shown to carry no apparent transit features within measurement precision. The distribution in detrended SAP flux measurements appears Gaussian-like. We attempted transit-curve fitting with informed and uninformed priors on the planetary radius, but this yielded no significant results. We applied a very similar methodology on detrended PDCSAP time-series of 20 s and of 2 min cadence – both proved equally unfruitful. On that account, we conclude that current TESS photometry strongly suggests that Barnard b is non-transiting. This implies a marginal constraint in orbital inclination of the planet ($i_b \leq 87.9^\circ$; 3σ). We were unable to find any other periodic darkening in the photometry timeseries that could be ascribed to planetary transits.

Acknowledgements. AKS acknowledges the support of a fellowship from the “la Caixa” Foundation (ID 100010434). The fellowship code is LCF/BQ/DI23/11990071. AKS, JIGH, ASM, CAP, NN, and RR acknowledge financial support from the Spanish Ministry of Science and Innovation (MICINN) project PID2020-117493GB-I00 and from the Government of the Canary Islands project ProID2020010129. NN acknowledges funding from Light Bridges for the Doctoral Thesis “Habitable Earth-like planets with ESPRESSO and NIRPS”, in cooperation with the Instituto de Astrofísica de Canarias, and the use of Indefeasible Computer Rights (ICR) being commissioned at the ASTRO POC project in Tenerife, Canary Islands, Spain. The ICR-ASTRONOMY used for his research was provided by Light Bridges in cooperation with Hewlett Packard Enterprise (HPE). ACG is funded by the Spanish Ministry of Science through MCIN/AEI/10.13039/501100011033 grant PID2019-107061GB-C61. AMS acknowledges support from the Fundação para a Ciência e a Tecnologia (FCT) through the Fellowship 2020.05387.BD (DOI: 10.54499/2020.05387.BD). Funded/Co-funded by the European Union (ERC, FIERCE, 101052347). Views and opinions expressed are however those of the author(s) only and do not necessarily reflect those of the European Union or the European Research Council. Neither the European Union nor the granting authority can be held responsible for them. This work was supported by FCT - Fundação para a Ciência e a Tecnologia through national funds by these grants: UIDB/04434/2020, UIDP/04434/2020. The work of CJAPM was financed by Portuguese funds through FCT (Fundação para a Ciência e a Tecnologia) in the framework of the project 2022.04048.PTDC (Phi in the Sky, DOI 10.54499/2022.04048.PTDC). CJAPM also acknowledges FCT and POCH/FSE (EC) support through Investigador FCT Contract 2021.01214.CEECIND/CP1658/CT0001 (DOI 10.54499/2021.01214.CEECIND/CP1658/CT0001). This paper includes data collected by the TESS mission, which are publicly available from the Mikulski Archive for Space Telescopes (MAST). Funding for the TESS mission is provided by NASA’s Science Mission Directorate. Resources supporting this work were provided by the NASA High-End Computing (HEC) Program through the NASA Advanced Supercomputing (NAS) Division at Ames Research Center for the production of the SPOC data products. We acknowledge the use of public TESS data from pipelines at the TESS Science Office and at the TESS Science Processing Operations Center. This research has made use of the Exoplanet Follow-up Observation Program website, which is operated by the California Institute of Technology, under contract with the National Aeronautics and Space Administration under the Exoplanet Exploration Program. This work made use of TESS-CONT, which builds upon `TPFPLOTTER` (Aller et al. 2020) and `TESS_PRF` (Bell & Higgins 2022). We used the following PYTHON packages for data analysis and visualisation: `ASTROPY` (Astropy Collaboration et al. 2022), `DYNESTY` (Speagle 2020) `LIGHTKURVE` (Lightkurve Collaboration et al. 2018), `LDTK` (Parviainen & Aigrain 2015; Husser et al. 2013), `MATPLOTLIB` (Hunter 2007), `NIEVA` (Stefanov et al., in prep.), `NUMPY` (Harris et al. 2020), `PANDAS` (McKinney 2010; The Pandas Development Team 2022), `PYASTRONOMY` (Czesla et al. 2019), `PYTRANSIT` (Parviainen 2015), `ScIPy` (Virtanen et al. 2020), `SEABORN` (Waskom 2021), `s+LEAF` (Delisle et al. 2020, 2022) and `WÖTAN` (Hippke et al. 2019). This manuscript was written and compiled in `OVERLEAF`. All presented analysis was conducted on `UBUNTU` machines.

References

- Akeson, R. L., Chen, X., Ciardi, D., et al. 2013, *Publications of the Astronomical Society of the Pacific*, 125, 989
- Aller, A., Lillo-Box, J., Jones, D., Miranda, L. F., & Barceló Forteza, S. 2020, *Astronomy and Astrophysics*, 635, A128
- Anglada-Escudé, G., Amado, P. J., Barnes, J., et al. 2016, *Nature*, 536, 437
- Astropy Collaboration, Price-Whelan, A. M., Lim, P. L., et al. 2022, *The Astrophysical Journal*, 935, 167
- Barnard, E. E. 1916, *The Astronomical Journal*, 29, 181
- Bell, K. J. & Higgins, M. E. 2022, *Astrophysics Source Code Library*, ascl:2207.008
- Castro-González, A., Lillo-Box, J., Armstrong, D. J., et al. 2024, *TOI-5005 b: A Super-Neptune in the Savanna near the Ridge*
- Crossfield, I. J. M., Petigura, E., Schlieder, J. E., et al. 2015, *The Astrophysical Journal*, 804, 10
- Czesla, S., Schröter, S., Schneider, C. P., et al. 2019, *Astrophysics Source Code Library*, ascl:1906.010
- Delisle, J. B., Hara, N., & Ségransan, D. 2020, *Astronomy and Astrophysics*, 638, A95
- Delisle, J.-B., Unger, N., Hara, N. C., & Ségransan, D. 2022, *Astronomy & Astrophysics*, 659, A182
- Gaia Collaboration, Vallenari, A., Brown, A. G. A., et al. 2022, *Gaia Data Release 3: Summary of the Content and Survey Properties*
- Gillon, M., Jehin, E., Lederer, S. M., et al. 2016, *Nature*, 533, 221
- González Hernández, J. I., Suárez Mascareño, A., Silva, A. M., et al. 2024, *Astronomy and Astrophysics*
- Harris, C. R., Millman, K. J., van der Walt, S. J., et al. 2020, *Nature*, 585, 357
- Hippke, M., David, T. J., Mulders, G. D., & Heller, R. 2019, *The Astronomical Journal*, 158, 143
- Hippke, M. & Heller, R. 2019, *Astronomy and Astrophysics*, 623, A39
- Hunter, J. D. 2007, *Computing in Science & Engineering*, 9, 90
- Husser, T.-O., Wende-von Berg, S., Dreizler, S., et al. 2013, *Astronomy & Astrophysics*, 553, A6
- Kinemuchi, K., Barclay, T., Fanelli, M., et al. 2012, *Publications of the Astronomical Society of the Pacific*, 124, 963
- Kopal, Z. 1950, *Harvard College Observatory Circular*, 454, 1
- Kovács, G., Zucker, S., & Mazeh, T. 2002, *Astronomy and Astrophysics*, 391, 369
- Lightkurve Collaboration, Cardoso, J. V. d. M., Hedges, C., et al. 2018, *Astrophysics Source Code Library*, ascl:1812.013
- McKinney, W. 2010, in *Python in Science Conference*, Austin, Texas, 56–61
- Mosteller, F. & Tukey, J. W. 1977, *Data Analysis and Regression: A Second Course in Statistics*, Addison-Wesley Series in Behavioral Science (Reading, Mass: Addison-Wesley Pub. Co)
- Murgas, F., Castro-González, A., Pallé, E., et al. 2023, *Astronomy and Astrophysics*, 677, A182
- Parviainen, H. 2015, *Monthly Notices of the Royal Astronomical Society*, 450, 3233
- Parviainen, H. & Aigrain, S. 2015, *Monthly Notices of the Royal Astronomical Society*, 453, 3822
- Parviainen, H., Luque, R., & Pallé, E. 2024, *Monthly Notices of the Royal Astronomical Society*, 527, 5693
- Rasmussen, C. E. & Williams, C. K. I. 2006, *Gaussian Processes for Machine Learning*, Adaptive Computation and Machine Learning (Cambridge, Mass: MIT Press)
- Ricker, G. R., Winn, J. N., Vanderspek, R., et al. 2015, *Journal of Astronomical Telescopes, Instruments, and Systems*, 1, 014003
- Savitzky, A. & Golay, M. J. E. 1964, *Analytical Chemistry*, 36, 1627
- Schweitzer, A., Passegger, V. M., Cifuentes, C., et al. 2019, *Astronomy & Astrophysics*, 625, A68
- Skilling, J. 2004, 735, 395
- Smith, J. C., Stumpe, M. C., Van Cleve, J. E., et al. 2012, *Publications of the Astronomical Society of the Pacific*, 124, 1000
- Speagle, J. S. 2020, *Monthly Notices of the Royal Astronomical Society*, 493, 3132
- Stumpe, M. C., Smith, J. C., Catanzarite, J. H., et al. 2014, *Publications of the Astronomical Society of the Pacific*, 126, 100
- Stumpe, M. C., Smith, J. C., Van Cleve, J. E., et al. 2012, *Publications of the Astronomical Society of the Pacific*, 124, 985
- Suárez Mascareño, A., González-Álvarez, E., Zapatero Osorio, M. R., et al. 2023, *Astronomy & Astrophysics*, 670, A5
- The Pandas Development Team. 2022, *Pandas-Dev/Pandas: Pandas*, Zenodo
- Virtanen, P., Gommers, R., Oliphant, T. E., et al. 2020, *Nature Methods*, 17, 261
- Waskom, M. 2021, *Journal of Open Source Software*, 6, 3021

¹Instituto de Astrofísica de Canarias, 38205 La Laguna, Spain

²Departamento de Astrofísica, Universidad de La Laguna, 38206 La Laguna, Spain

³Light Bridges S. L., 35004 Las Palmas de Gran Canaria, Spain

⁴Consejo Superior de Investigaciones Científicas (CSIC), 28006 Madrid, Spain

⁵INAF - Osservatorio Astrofisico di Torino, Via Osservatorio 20, 10025 Pino Torinese, Italy

⁶Centro de Astrobiología (CAB), CSIC-INTA, ESAC campus, Camino Bajo del Castillo s/n, 28692 Villanueva de la Cañada, Spain

⁷Instituto de Astrofísica e Ciências do Espaço, CAUP, Universidade do Porto, Rua das Estrelas, 4150-762 Porto, Portugal

⁸Departamento de Física e Astronomia, Faculdade de Ciências, Universidade do Porto, Rua do Campo Alegre, 4169-007 Porto, Portugal

⁹Instituto de Astrofísica e Ciências do Espaço, Faculdade de Ciências da Universidade de Lisboa, Campo Grande, 1749-016 Lisboa, Portugal

¹⁰Centro de Astrofísica da Universidade do Porto, Rua das Estrelas, 4150-762 Porto, Portugal

*e-mail: atanas.stefanov@iac.es

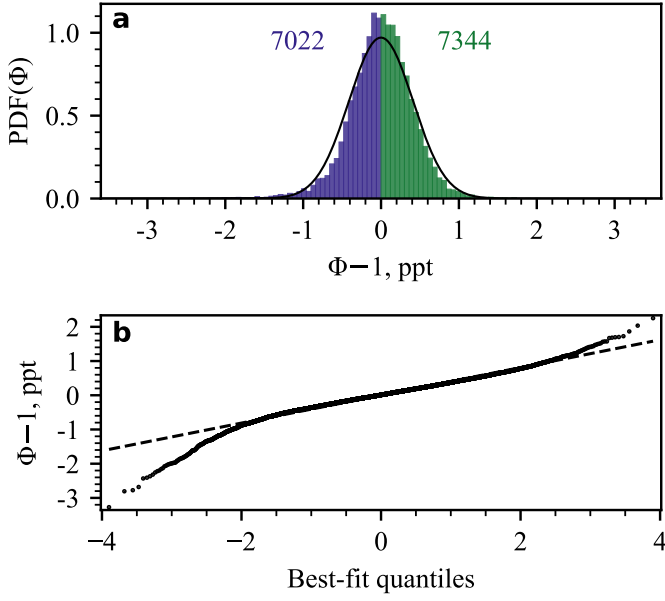


Fig. A.1. (a) Distribution plot of detrended PDSCAP photometry. The distribution is conventionally split in two to a lower distribution (blue bars) and an upper distribution (green bars). The size of these sub-distributions are given in figures of corresponding colour. A Gaussian-function fit to the distribution is given in a black solid line. (b) Probability plot assessing whether the full distribution (black solid line) follows the fitted Gaussian (black dashed line).

Appendix A: Supplementary material

Table A.1. Relevant parameters of Barnard b and planetary candidates from the four-planet solution in González Hernández et al. (2024).

Symbol	Unit	Value	Ref.
Barnard b			
a_b	au	0.0229(3)	1
P_b	d	3.1537(5)	1
$T_{0,b} - 2\,460\,000$	d	139.290 ± 0.104	1
$M_b \sin i_b$	M_\oplus	0.32 ± 0.04	1
R_b	R_\oplus	0.73 ± 0.04	0
D_b	ppt	$1.42^{+0.23}_{-0.26}$	0
W_b	h	$0.82^{+0.11}_{-0.27}$	0
Barnard c (cand.)			
a_c	au	0.0274(4)	1
P_c	d	4.1243(8)	1
$T_{0,c} - 2\,460\,000$	d	139.730 ± 0.129	1
$M_c \sin i_c$	M_\oplus	0.31 ± 0.04	1
R_c	R_\oplus	0.72 ± 0.04	0
D_c	ppt	$1.40^{+0.23}_{-0.25}$	0
W_c	h	$0.89^{+0.12}_{-0.30}$	0
Barnard d (cand.)			
a_d	au	0.0188(3)	1
P_d	d	2.3407(4)	1
$T_{0,d} - 2\,460\,000$	d	138.458 ± 0.101	1
$M_d \sin i_d$	M_\oplus	0.22 ± 0.03	1
R_d	R_\oplus	0.65 ± 0.04	0
D_d	ppt	$1.12^{+0.20}_{-0.21}$	0
W_d	h	$0.74^{+0.10}_{-0.25}$	0
Barnard e (cand.)			
a_e	au	0.0381(6)	1
P_e	d	6.7377(56)	1
$T_{0,e} - 2\,460\,000$	d	137.405 ± 0.551	1
$M_e \sin i_e$	M_\oplus	0.17 ± 0.05	1
R_e	R_\oplus	$0.62^{+0.08}_{-0.05}$	0
D_e	ppt	$1.01^{+0.31}_{-0.21}$	0
W_e	h	$1.05^{+0.14}_{-0.35}$	0

References. (0) This work; (1) González Hernández et al. (2024).

Notes. The expected radius, transit depth and transit width were naïvely computed under two assumptions: (i) that Barnard b follows the mass-radius relation provided by Parviainen et al. (2024); (ii) that the impact parameter follows the uniform distribution $\mathcal{U}(0, 1)$. Reported uncertainties reflect the 16th and the 84th percentiles. Some uncertainties are given in parentheses, to the order of the least significant figure.

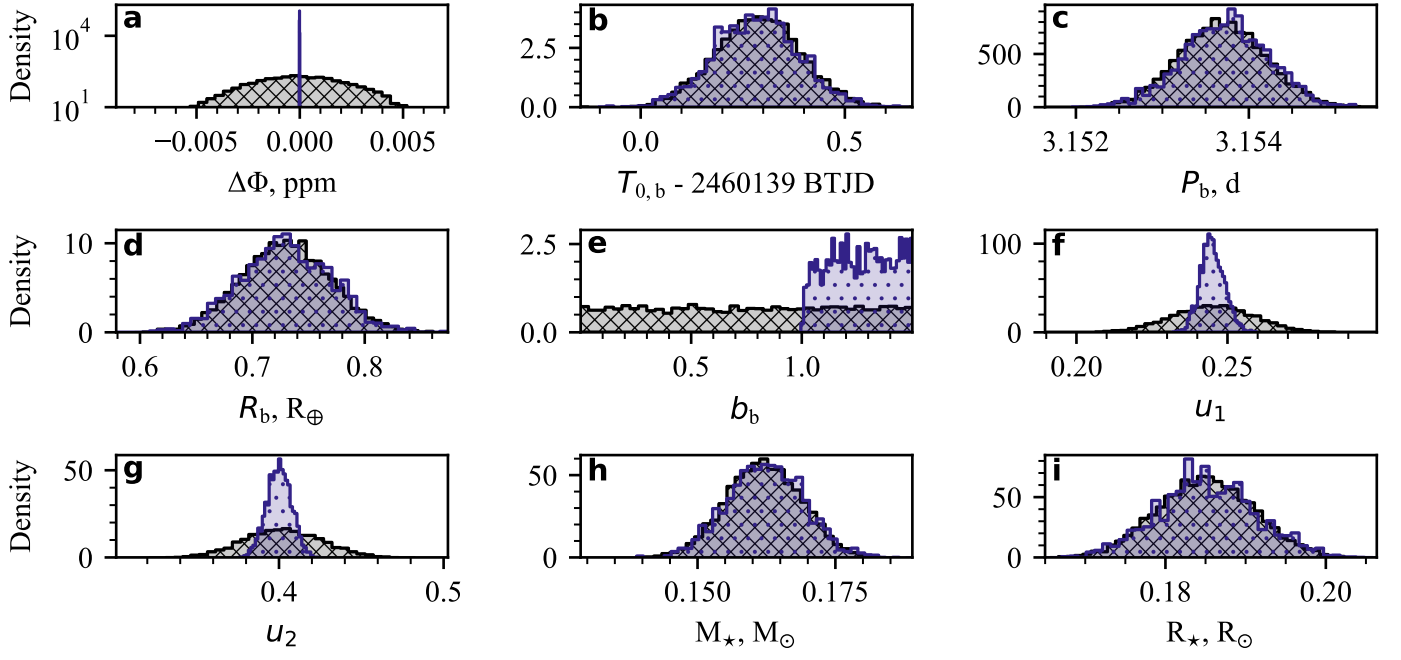


Fig. A.2. Prior (black, cross-hatched) and posterior (blue, dot-hatched) parameter distributions in our narrow-prior radius search of Barnard b.